LAWRENCE
LIVERMORE
NATIONAL
LABORATORY

UCRL-JRNL-155696

Controlling Surface Roughness in Vapor Deposited Poly(amic acid) Films by Solvent-Vapor Exposure

M. Anthamatten, S. A. Letts, and R. C. Cook

November 4, 2003

Langmuir Journal

Updated October 14, 2003

Controlling Surface Roughness in Vapor-Deposited Poly(amic acid) Films by Solvent-Vapor Exposure

Mitchell Anthamatten,*,† Stephan A. Letts, and Robert C. Cook
Lawrence Livermore National Laboratory, P.O. Box 808, M.S. L-474, Livermore, California 94550

A series of vapor-deposited poly(amic acid) (PAA) films were exposed to dimethyl sulfoxide (DMSO) vapors to investigate sorption kinetics and surface smoothing phenomena. Gravimetric sorption and secondary-ion mass spectrometry (SIMS) results are both consistent with frontal (case II) diffusion. These experiments suggest that the solvent front is defined by a sharp interface that delineates the swollen material from the unswollen material. Solvent-vapor smoothing was studied by first depositing PAA onto rough aluminum surfaces, and then, during solvent-vapor exposure, the surface topology was continuously monitored using a light interference microscope. The resulting time-dependent power spectra indicate that high-frequency defects smooth faster than low-frequency defects. This frequency dependence was further investigated by depositing PAA onto a series of sinusoidal surfaces and exposing them to solvent vapor inside a flow channel. The sinusoidal amplitudes decay exponentially with time, with decay constants that are proportional to the surface frequency. To explain the physics of surface smoothing, a two-parameter model is presented and agrees qualitatively with experimental data.

Introduction

Ultrasmooth polymer films are of great importance in a large body of technical applications, e.g., optical coatings,[1,2] super mirrors, waveguides, paints, and inertial confinement fusion targets.[3-5] Surface roughness typically originates during processing steps as solvent is removed. For example, the roughness of spin-coated films depends on the volatility of the solvent used.[6,7] To obtain smooth surfaces, polymer films are typically annealed well above their glass transition temperature.[8-11] At these temperatures polymers are liquid-like, and surface flattening is driven by primarily interfacial tension and involves diffusive[1] or viscous mass transport.

Several techniques have recently been applied to study roughness and surface smoothing of polymer surfaces, including AFM, laser diffraction,[12] ellipsometry, X-ray scattering,[1,7] and birefringence techniques.[11,13] Most of these studies were carried out on thin films; however, when studying smoothing phenomena, the presence of the underlying substrate can be undesirable. From a practical standpoint, correlated substrate roughness and contamination can complicate measurements. Also, polymer melts have been shown to exhibit heightened viscosities in confined environments,[14] and the mismatch in the thermal expansion coefficient between the substrate and the polymer sample may lead to additional film stresses.

The dynamics of surface smoothing depends on the length scale of surface features. Li et al.[1] have measured the time dependence of surface corrugation amplitudes during annealing of polystyrene and poly(methyl methacrylate) thin films. By comparing the rate of amplitude decay for surfaces with different corrugation frequencies, the authors confirmed mass transport was dominated by surface diffusion and were able to determine a surface diffusion coefficient. Hamdorf and Johannsmann[12] also studied the relaxation of imprinted surface corrugation gratings to determine surface rheological properties. They found near-surface moduli agree with bulk values, whereas stiffness was significantly larger near the surface. In both of these efforts, well-defined surface topologies were fabricated with vertical features on the order of 10 nm; during annealing, the decay of these surface features was monitored. This enables the frequency dependence of smoothing to be investigated.

Unfortunately, many glassy polymer systems exhibit very high glass transition temperatures, and from a processing standpoint, annealing may be impractical. An alternative approach to obtaining smooth surfaces is to temporarily swell the polymer film by exposing it to solvent vapor, enabling viscous flow to occur beneath the surface. This solvent-smoothing process is shown schematically in Figure 1. In the swollen state, surface forces overwhelm viscous forces, and smooth polymer films can be obtained.

† Present address: University of Rochester, Department of Chemical Engineering, 206 Gavett Hall, Rochester, NY, 14627.
* Corresponding author: Tel (585) 273-5526; Fax (585) 273-1348; e-mail anthamatten@che.rochester.edu.

(1) Li, Z.; Tolan, M.; Hoehr, T.; Kharas, D.; Qu, S.; Sokolov, J.; Rafailovich, M. H.; Lorenz, H.; Kotthaus, J. P.; Wang, J.; Sinha, S. K.; Gibaud, A. *Macromolecules* **1998**, *31*, 1915-1920.
(2) Feng, Y. P.; Sinha, S. K.; Deckman, H. W.; Hastings, J. B.; Siddon, D. P. *Phys. Rev. Lett.* **1993**, *66*, 2108.
(3) Haan, S. W.; Dettrich, T.; Strobel, G. L.; Hatchett, S.; Hinkel, D.; Marinak, M.; Munro, D.; Jones, O.; Pollaine, S. M.; Suter, L. *Fusion Technol.* **2002**, *41*, 164-173.
(4) Haan, S. W.; Pollaine, S. M.; Lindl, J. D.; Suter, J. L.; Berger, R. L.; Powers, L. V.; Alley,W.E.; Amendt, P. A.; Futterman, J. A.; Levedahl, W. K.; Rosen, M. D.; Rowley, D. P.; Sacks, R. A.; Shestakov, A. I.; Strobel, G. L.; Tabak, M.; Weber, S. V.; Zimmerman, G. B.; Krauser, W. J.; Wilson, D. C.; Coggeshall, S. V.; Harris, D. B.; Hoffman, N. M.; Wilde, B. H. *Phys. Plasmas* **1995**, *2*, 2480-2487.
(5) Lindl, J. *Phys. Plasmas* **1995**, *2*, 3933-4373.
(6) Strawhecker, K. E.; Kumar, S. K.; Douglas, J. F.; Karim, A. *Macromolecules* **2001**, *34*, 4669-4672.
(7) Mueller-Buschbaum, P.; Gutmann, J. S.; Wolkenhauer, M.; Krause, J.; Stamm, M.; Smilgies, D.; Petry, W. *Macromolecules* **2001**, *34*, 1369-1375.
(8) Dubas, S. T.; Schlenoff, J. B. *Langmuir* **2001**, *17*, 7725-7727.
(9) Goh, M. C.; Juhue, D.; Leung, O. M.; Wang, Y.; Winnik, M. A. *Langmuir* **1993**, *9*, 1319-1322.
(10) Park,Y. J.; Lee, D. Y.;Khew,M.C.;Ho, C. C.;Kim, J.H.*Langmuir* **1998**, *14*, 4972-4977.
(11) Schwab, A. D.; Agra, D. M. G.; Kim, J. H.; Kumar, S.; Dhinojwala, A. *Macromolecules* **2000**, *33*, 4903-4909.
(12) Hamdorf, M.; Johannsmann, D. *J. Chem. Phys.* **2000**, *112*, 4262-4270.
(13) Pu, Y.; White, H.; Rafailovich, M. H.; Sokolov, J.; Schwarz, S. A.; Dhinojwala, A.; Agra, D. M. G.; Kumar, S. *Macromolecules* **2001**, *34*, 4972-4977.
(14) Hu, H. W.; Granick, S. *Science* **1992**, *258*, 1339-1341.

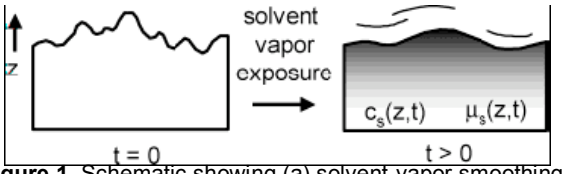

Figure 1. Schematic showing (a) solvent-vapor smoothing of a rough surface and (b) sintering of two free-standing films. During solvent exposure, solvent concentration and viscosity are position- and time-dependent.

viscous forces, and smooth polymer films can be obtained. During solvent-vapor exposure a concentration profile develops in which the solvent concentration is depth- and time-dependent. Likewise, for glassy polymer systems, the viscosity, η, is also depth- and time-dependent and is related to polymer concentration, c_p, through a power law relationship.[15,16]

The efficacy of the surface smoothing process should be highly sensitive to sorption and diffusion kinetics. If solvent-vapor sorption is slow compared to the time scales of flow, then mass transfer will primarily occur near the surface. If, however, solvent-vapor sorption is fast compared to viscous flow relaxation times, then mass transfer may occur well beneath the surface. Furthermore, smoothing kinetics will depend on the mechanism of solvent vapor sorption, the relationship between solvent concentration and the viscosity of the swollen layer, and the shape and size of the surface defect being smoothed.

In this paper, we report on the sorption and smoothing phenomena observed in vapor-deposited poly(amic acid) (PAA) films following exposure to dimethyl sulfoxide vapor. Films examined here are thicker than those examined in earlier studies, and the roughness features studied are more than an order of magnitude larger than the characteristic length scale of the polymer molecules. Poly-(amic acid)s can be thermally cured to form polyimides, which are well-known for their thermal and mechanical properties. These polyimides are candidate materials for inertial confinement fusion (ICF) laser targets being developed at the Lawrence Livermore National Laboratory[17-20] and elsewhere.[21,22] Here, control of surface roughness is essential to preclude Rayleigh-Taylor instabilities that develop during laser ablation.[4,5]

Experimental Section

Vapor deposition of 4,4'-oxydianiline (ODA) and pyromellitic dianhydride (PMDA) monomers to form poly(amic acid) films was performed at pressures ~10^{-6} Torr inside a custom-built deposition chamber. Experimental details relevant to this process are provided elsewhere.[17] This technique offers good control over material composition and film thickness.

Mass uptake measurements were made with a Cahn 2000 recording electrobalance. The balance was mounted in a glass solvent exposure chamber with connections to an inlet exposure gas supply, a nitrogen purge stream (to prevent solvent condensation on the balance), and an outlet vent. Samples were suspended from the balance in an stainless steel hang-down assembly at the bottom of a 45 cm platinum wire. At this position, samples only contacted the inlet exposure gas. The exposure gas consisted of a 100 mL/min flow of dry nitrogen that had been passed through a gas sparger immersed into pure DMSO. A liquid nitrogen cold trap was used to verify the composition of the inlet stream to be >96% relative DMSO vapor saturation, calculated according to the Antoine equation.[23] Extra dry nitrogen was mixed with the saturated gas stream to achieve lower levels of relative saturation. Samples consisted of 20-100 μm thick poly(amic acid) films deposited onto 6.5 mm diameter aluminum disks. Sample weights ranged from 2 to 10 mg, and the electrobalance could detect changes as small as 1 μg.

Secondary ion mass spectroscopy was done with a CAMECA IMS 3F instrument with a negative Cs primary beam (7-23 nA) of about 35 μm diameter rastered over an area of 75 μm × 75 μm.

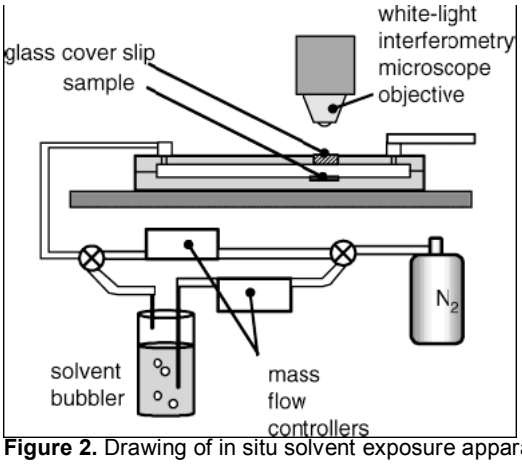

Figure 2. Drawing of in situ solvent exposure apparatus.

The sputtering of the sample by the primary beam produces a crater in the film. The edges of the crater may be irregular, so to avoid difficulties in data interpretation, only the central 60 μm diameter region of the secondary ion beam was analyzed. During sputtering, the ejected secondary ions accurately reflect the composition of the surface, and as successive layers are etched away, the data acquired represent a quantitative depth profile of each atomic ion encountered. Data were collected for the following elements: ^{12}C, ^{16}O, $^{26}(CN)$, ^{32}S, $^{32}O_2$, ^{34}S. Counting times were 10 s at each mass station.

Smoothing experiments were carried out in a custom-built solvent-exposure chamber shown in Figure 2. A stream of dry nitrogen was first bubbled through liquid DMSO, and then, to control the relative concentration of DMSO vapor, this stream could be combined with additional dry nitrogen. The combined gas stream then contacts the sample inside the solvent exposure chamber, which is mounted onto a microscope stage. The cross sectional dimensions of the exposure channel were machined to be 14.6 × 2.0 mm. Experiments were performed using gas flow rates of 50, 100, and 200 mL/min; these flow rates correspond to Reynolds numbers of *Re*) 2.7, 5.4, and 10.8, respectively. During solvent exposure, a white-light interference microscope (WYKO HD-2000) was used to characterize sample surfaces. A glass coverslip was used to cover the sample between microscope scans. Topological data were obtained through none contact vertical scanning interferometry; this technique involves the measurement of the degree of fringe modulation at varying objective to-sample distances.[24,25]

Results and Discussion

Sorption Studies. Sorption experiments will first be discussed in order to investigate how a solvent (DMSO) concentration profile develops in poly(amic acid) films. Gravimetric sorption data were acquired at room temperature for samples exposed to inlet gas streams with

(15) Berry, G. C. *J. Rheol.* **1996**, *40*, 1129-1154.
(16) Kelley, F. N.; Bueche, F. *J. Polym. Sci.* **1961**, *L*, 549-556.
(17) Roberts, C. C.; Letts, S. A.; Saculla, M. D.; Hsieh, E. J.; Cook, R. C. *Fusion Technol.* **1999**, *35*, 138-146.
(18) Roberts, C. C.; Orthion, P. J.; Hassel, A. E.; Parrish, B. K.; Buckley, S. R.; Fearon, E.; Letts, S. A.; Cook, R. C. *Fusion Technol.* **2000**, *38*, 94-107.
(19) Letts, S. A.; Nissen, A. E.; Orthion, P. J.; Buckley, S. R.; Fearon, E.; Chancellor, C.; Roberts, C. C.; Parrish, B. K.; Cook, R. C. *Fusion Technol.* **2002**, *41*, 268-277.
(20) Letts, S.; Anthamatten, M.; Buckley, S.; Fearon, E.; Nissen, A. E.; Cook, R. Submitted to *Fusion Technol*.
(21) Alfonso, E. L.; Tsai, F. Y.; Chen, S.-H.; Gram, R. Q.; Harding, D. R. *Fusion Technol.* **1999**, *35*, 131-137.
(22) Tsai, F. Y.; Harding, D. R.; Chen, S. H.; Alfonso, E. L. *Fusion Technol.* **2002**, *41*, 178.
(23) Riddick, J. A.; Bunger, W. B.; Sakano, T. K. *Organic Solvents*s *Physical Properties and Methods of Purification*, 4th ed.; John Wiley & Sons: New York, 1986.
(24) Caber, P. J. *Appl. Opt.* **1993**, *32*, 3438-3441.
(25) Wyant, J. C. *Laser Focus World* **1993** (Sept), 131-133.
(26) Thomas, N. L.; Windle, A. H. *Polymer* **1981**, *23*, 529-542.

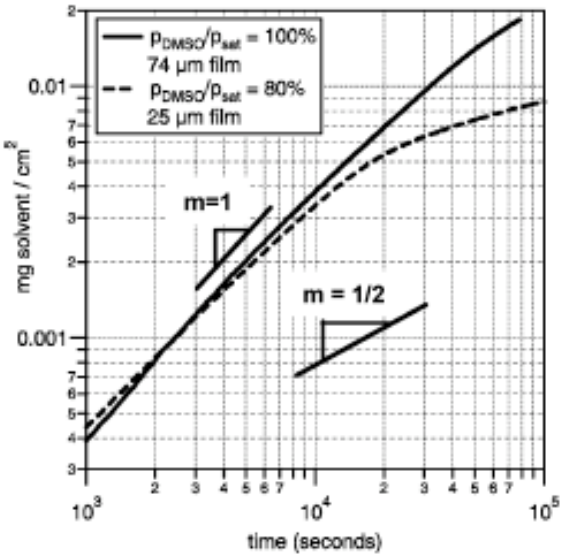

Figure 3. Gravimetric sorption DMSO into PAA films at early times. Data are plotted as solvent uptake permm$_2$ of film area vs time.

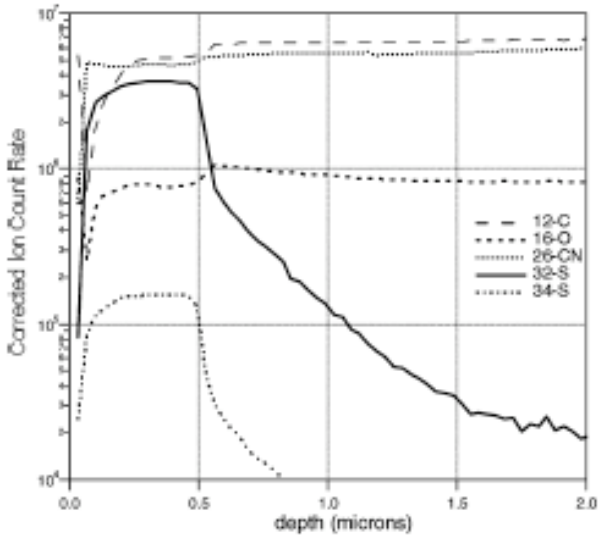

Figure 4. Ion microscope depth profiles of a poly(amic acid) film following exposure to nearly saturated DMSO vapors for 5 min.

different values of relative saturation. For vapor streams with low DMSO compositions (p_{DMSO}/p_{sat}<0.4) little or no sorption was observed. Figure 3 shows two sorption curves on a logarithmic plot taken from PAA films exposed to gas streams at high levels of DMSO saturation. Since these films differ in thickness (25 and 74 μm for p_{DMSO}/p_{sat} = 0.8 and 1.0, respectively), mass gains have been normalized by the film's surface area. At early times sorption curves agree with each other, indicating that the sorption rate is independent of film thickness, and at high enough levels of saturation, the rate of sorption is nearly independent of DMSO partial pressures. For both curves, the rate of solvent sorption begins to plateau when the solvent propagation front reaches the back of the film.

The data in Figure 3 indicate that solvent transport through the poly(amic acid) is non-Fickian. For Fickian diffusion, one would expect proportionality between the mass uptake and the square root of time; this would result in a slope of m = 1/2 on the logarithmic scale in Figure 3. Instead, the data agree more closely with case II diffusions a second, limiting transport mechanism that is frequently observed in a variety of glassy polymer systems.[26-28] Case II diffusion can be explained on the basis of a glassy polymer's retarded viscous response to local changes in the fluid's chemical potential. In case II diffusion, upon reaching a critical surface concentration, a sharp concentration front develops and propagates into the polymer bulk at a nearly constant speed, and behind the advancing front the swollen polymer is in an equilibrium state of swelling and should be free of concentration gradients. According to this mechanism, upon exposure to solvent vapor one would expect the sample's mass to increase linearly with time as is observed experimentally (m = 1 in Figure 3). Also, the experimental observation that no sorption occurs under a critical gas stream composition agrees with the phenomenology of case II diffusion.[27] It is, however, somewhat surprising that the rate of solvent uptake is only weakly correlated to the DMSO vapor pressure. This implies that the solvent front velocity is nearly independent of the activity of the swollen layer.

The most convincing evidence of case II diffusion is revealed in the SIMS data. The sulfur atom, not present in the as-deposited polymer, is used as a tag on the DMSO molecules, and we can unambiguously determine the solvent concentration profile. Pinto et al.[29] first employed SIMS in a fashion similar to study aqueous dye diffusion through water-soluble copolymers. Figure 4 shows the elemental concentration profiles obtained from SIMS following 5min of saturated DMSO vapor exposure (p_{DMSO}/p_{sat} = 1.0). These experiments were performed at room temperature. Clearly, there is a well-defined depth (~0.5 *í*m) at which all the monitored elemental concentrations show an abrupt change. This depth marks the edge of the solvent penetration front. From these data alone, it is not clear whether there is an induction period, before any solvent enters the film, or whether the solvent velocity is linear, as the sorption experiments suggested, over the entire 5 min exposure time. Similar experiments were performed on samples exposed to 15 min of solvent vapor, and the position of the front measured using SIMS was roughly 3 times (~1.5 μm) as deep as that observed in films exposed for 5 min. This result is consistent with the time-linear mass uptake results shown in Figure 3 and suggests that the front velocity is almost constant under the conditions examined here.

Behind the solvent front, i.e., near the surface of the film, the C, O, and CN count rates all exhibit slightly lower signals (by 10-20%) than they do in the bulk. This reinforces the idea that the surface layer is swollen with a substance that has a lower mass fraction of these elements. Sulfur, on the other hand, is only present in the solvent, and thus the ^{32}S and ^{34}S profiles directly correspond to the solvent-concentration profile. Behind the front there is a nearly uniform level of sulfur presents except for within 100 nm of the film's surface where some solvent was presumably lost during sample preparation. Ahead of the front, the sulfur signal rapidly decays by over 2 decades. It appears that a small amount of solvent

(27) Alfrey, T.; Gurnee, E. F.; Lloyd, W. G. *J. Polym. Sci., Part C* **1966**, *12*, 249-261.
(28) Hassan, M. M.; Durning, C. J. *J. Polym. Sci., Part B: Polym. Phys.* **1999**, *37*, 3159-3171.
(29) Pinto, J. R.; Novak, S. W.; Nicholas, M. *J. Phys. Chem. B* **1999**, *103*, 8026-8032.

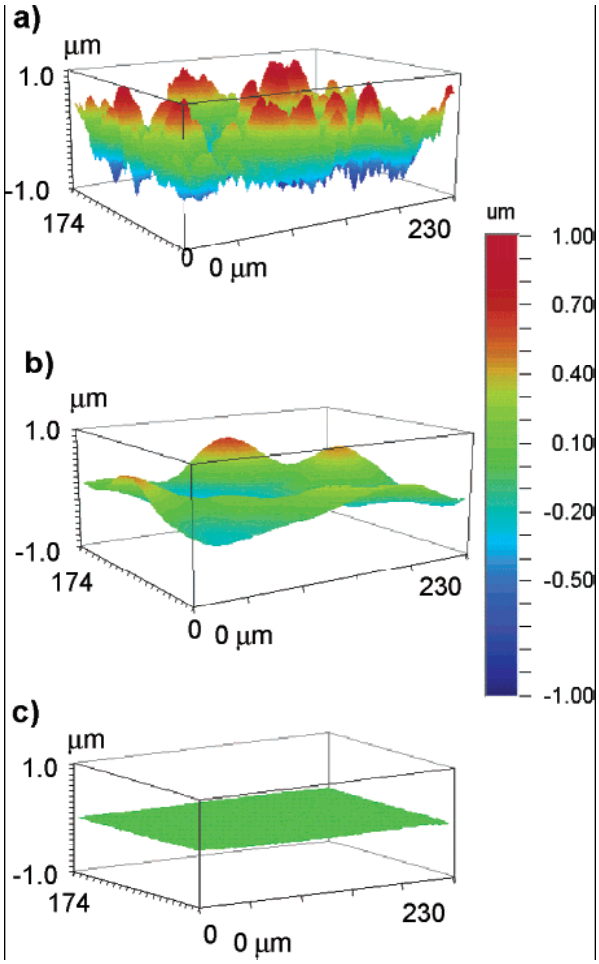

Figure 5. White-light interferometry images of poly(amic acid) deposited onto a rough aluminum surface. Image (a) was taken prior to solvent treatment, and (b) and (c) were taken following 15 and 80 min, respectively, of DMSO-vapor exposure.

penetrates into the film prior to the front movement. Others have predicted[26] and observed[30] such "Fickian precursors" in glassy polymer systems. Following a few of the SIMS measurements, films were allowed to sit in the vacuum chamber for 6 h. A second SIMS was then acquired, and the shape and magnitude of all the elemental profiles did not change significantly. This suggests that the propagation of the solvent front further into the poly-(amic acid) film is related to the interfacial mass transfer of DMSO from the vapor phase to the swollen layer.

Surface Smoothing. The main objective of this work is to investigate how the presence of a DMSO-rich surface layer affects the surface features of vapor-deposited PAA films. We shall start by describing the smoothing of an initially rough polymer film, and then we will examine how smoothing kinetics depend on defect size by studying a series of patterned surfaces.

Rough poly(amic acid) surfaces were obtained by vapor-depositing 30 μm of coating onto rough aluminum surfaces. The as-deposited surface, shown in Figure 5a, exhibits about the same roughness (~350 nm) as the bare aluminum surface (not shown). The surface roughness was significantly reduced during solvent-vapor exposure, as indicated in Figure 5b,c. The images in Figure 5 were acquired in situ during solvent-vapor exposure using a nearly saturated DMSO vapor stream at a flow rate of 250 mL/min. Each image was acquired from the same

(30) Gall, T. P.; Lasky, R. C.; Kramer, E. J. *Polymer* **1990**, *31*, 1491-1499.

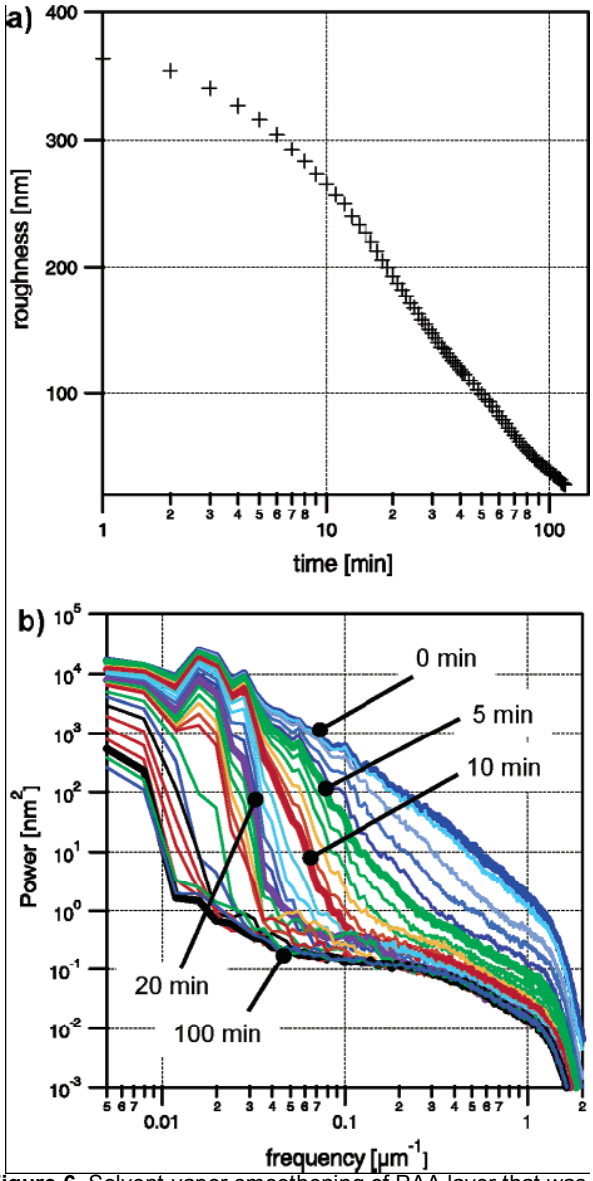

Figure 6. Solvent-vapor smoothening of PAA layer that was vapor-deposited onto a rough (~350 nm) aluminum surface: (a) plot of surface roughness vs time during solvent exposure; (b) evolution of the 1D surface power spectrum. The data for both figures were calculated from raw in situ interferometric microscopy images like those shown in Figure 5.

area of the sample at different exposure times. A total of 80 such snapshots were taken of this particular surface. Each image is a digital representation of a 736 × 480 pixel array of height data. The raw interferometry data can be used to calculate the root-mean-squared of roughness, which is plotted versus the natural logarithm of time in Figure 6a. Following an induction period the process is nearly exponential—the surface roughness decreases in a smooth, monotonic manner from 375 nm at t = 0 min to less than 25 nm at t = 120 min.

To examine the frequency dependence of the roughness, power spectra were calculated[31] from the raw interferometry data. This was done by first calculating the Fourier transform of each of the 480 data rows (736 pixels long). The corresponding power spectrum for each row was

(31) Press, W. H.; Teukolsky, S. A.; Vetterling, W. T.; Flannery, B. P. *Numerical Recipes in C: The Art of Scientific Computing*; Cambridge University Press: Cambridge, 1992.

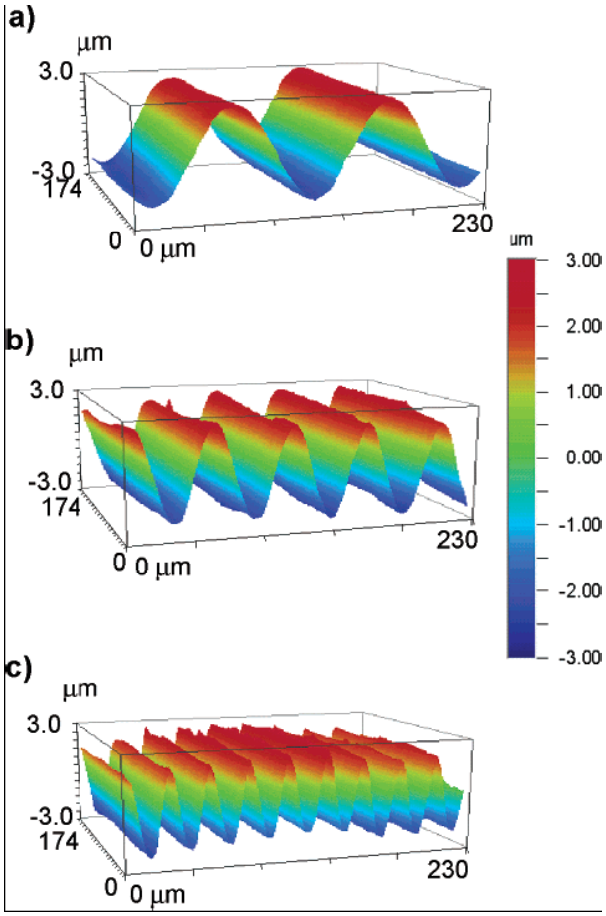

Figure 7. White-light interferometry images of three precision machined sinusoidal surfaces after (a-c) vapor deposition of poly(amic acid) coatings. The wavelength and amplitude features of the underlying substrate are fully retained though the deposition process.

calculated by squaring the resulting Fourier coefficients. All the resulting 1D power spectra were then averaged to determine a representative power spectrum, plotted as a function of frequency, for the 174 230 μm patch. Figure 6b shows the evolution of the power spectra during solvent exposure for the poly(amic acid) film discussed above. Prior to solvent exposure, the arbitrarily rough surface showed roughness at nearly all frequencies. The small peak at about 0.02 μm^{-1} indicates a dominant in-plane length that likely arises machine marks present in the underlying aluminum substrate. As expected, smoothing kinetics exhibit a strong frequency dependence. The high-frequency roughness (>0.1 μm^{-1}) decreases rapidly (<10 min), whereas the low-frequency roughness (<0.05 μm^{-1}) persists even after long exposure times. To more rigorously study the frequency dependence of smoothing, we studied the smoothing of poly(amic acid) over well-defined sinusoidal patterns that were precision machined into flat copper surface. The three sinusoidal surfaces had identical amplitudes of 5 μm but different periods (λ) 100, 50, and 25 μm). Figure 7a-c shows the sinusoidal surfaces following vapor deposition of 30 μm of PAA. This thickness is large compared to the surface amplitude; thus, surface smoothing should be decoupled from the patterns on the underlying substrate. Clearly, the surface features on the coatings were maintained throughout vapor deposition.

All three sinusoidal surfaces were simultaneously exposed to saturated DMSO vapor, and surface images

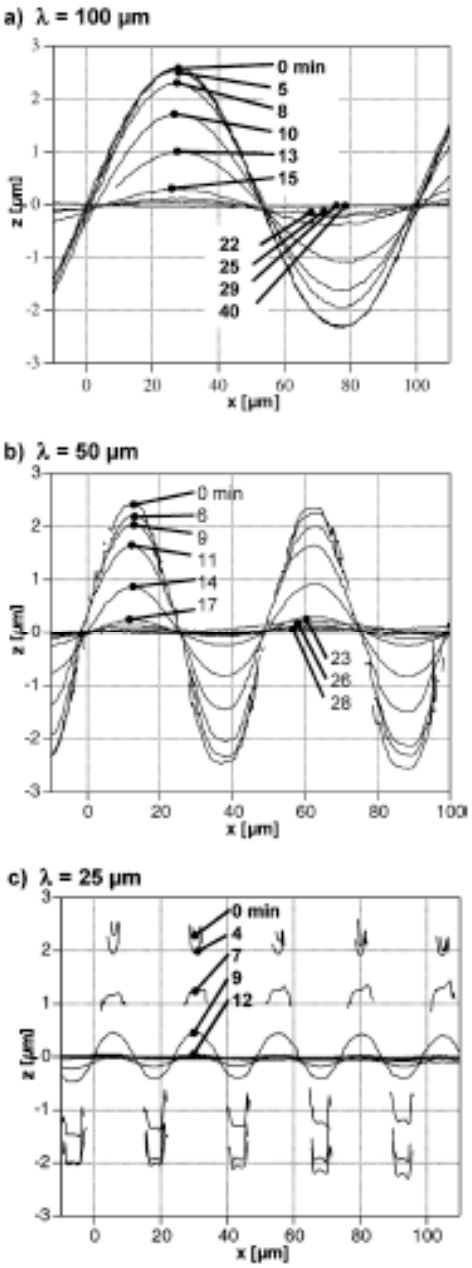

Figure 8. Examples of white-light interferometry 1-D profiles of sinusoidal surfaces during in situ solvent-vapor smoothing at a flow rate of 200 cm^3/min.

were acquired every few minutes. This experiment was repeated using several different gas flow rates: 50, 100, and 200 cm^3/min. Figure 8a-c shows examples of the 1D interferometry profiles of the evolving surfaces acquired during DMSO-vapor exposure. Some points on these scans, between the peaks and valleys, were not resolvable through interferometry and were dropped. This is especially apparent in Figure 8c. The maximum surface slope that can be measured by the microscope is limited by the resolution of the optical system and the pixel spacing of the detector array.[24] The data that have very low values of fringe modulation are therefore invalidated. However, the surface crest-to-crest amplitudes can clearly be obtained.

From the line profiles of the sinusoidal surface, like those shown in Figure 8, the surface amplitude can be

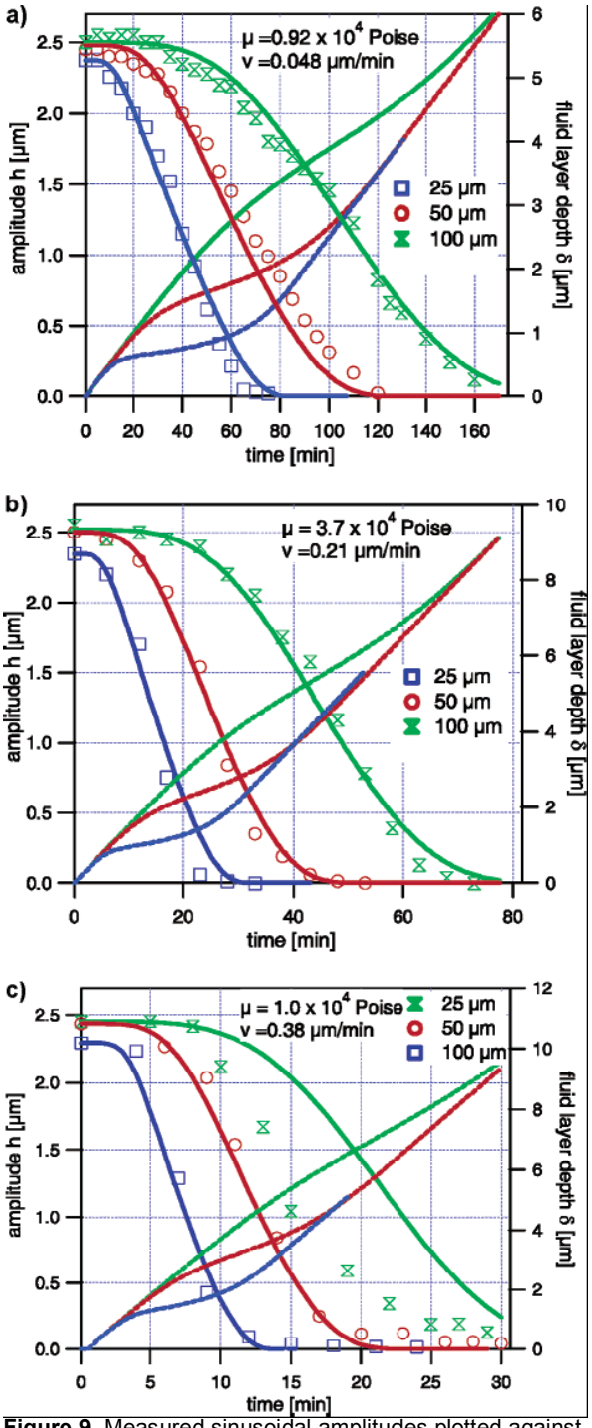

Figure 9. Measured sinusoidal amplitudes plotted against time for experiments conducted at (a) 50, (b) 100, and (c) 200 cm^3/min. Solid lines represent fits to the falling film model using the parameters shown in the figure. Upward-sloping lines are read using the right-hand axis and denote the model's prediction of the fluid layer thickness.

calculated by averaging several heights and valley depths. Figure 9 shows the sinusoidal amplitudes (open symbols, left axis) plotted against time for each flow rate and for each type of surface studied. At early times (<5 min), very little smoothing occurs. This induction time may be due to the fact that solvent has not penetrated deep enough into the polymer to permit significant flow. Most of the smoothing occurs during intermediate times, where the surface amplitude decreases by over a factor of 10. At long times the amplitude asymptotically approaches zero. Higher gas flow rates lead to faster smoothing, and for each flow rate examined the higher-frequency surfaces smooth faster than the lower-frequency surfaces. The solid lines in Figure 9 are fits obtained using the physical model described in the following section.

Modeling the Physics of Surface Smoothing. In this section we present a physical model to describe the data presented in Figure 9a-c. This model is based on the very well-established falling-film model;[32,33] however, differences in surface pressure will drive flow instead of gravity. To begin, consider the sinusoidal surface shown in Figure 10 that can be mathematically described by $W(x) = h_0 \sin\omega(x)$. Note that the positive z-direction is taken as downward(into the film) since the solvent will penetrate in that direction. We use the limit of case II diffusion to define the solvent concentration profile perpendicular to the surface. As solvent penetrates into the material, a swollen layer develops that has a thickness δ that is increasing at a constant rate defined by the frontal velocity v_f. The swollen layer is assumed to have a uniform solvent concentration c and a constant fluid viscosity μ Beneath the swollen layer the solvent concentration is set to zero. Pressure differences within the swollen layer drive mass transport. The pressure within the swollen layer is approximated using the Laplace-Young equation (typically used to describe the pressure drop across a fluid interface):

$$P_{\ddot{a}}(x) \;) \; P_{\text{ext}} - 2\varsigma K \qquad (1)$$

Where P_{ext} is the external pressure, γ is the surface tension at the air interface, and K is the mean curvature of the surface. The local mean curvature of the sinusoidal surface is defined according to the conventional definition as

$$K = \left[1 + \left(\frac{\partial W(x)}{\partial x}\right)^2\right]^{-3/2} \frac{\partial^2 W(x)}{\partial x^2} \qquad (2)$$

Initially, we shall only consider pressure gradients and mass transfer in the x-direction. This is a reasonable assumption as long as the fluid layer thickness is small compared to the length scale of flow ($1/\omega$) observed during the experiment. Effects of gravity are neglected.
To study the decay of a single sinusoidal bump, we consider two points on the surface: one at the crest of the bump x_c and one a small distance ϕx away from the crest. During smoothing, the swollen layer becomes thinnest at a crest since mass is continuously being transferred into the adjacent valleys. Furthermore, the local pressure differences in the swollen layer that will drive fluid flow (arising from differences in surface curvature) are smallest here, i.e., $\partial K/\partial x = 0$ at $x = \pi/2$. For both of these reasons, the choice of modeling the surface at a crest is crucial because here mass transfer is slowest and limits the amplitude decay dynamics. On the basis of a differential change in surface curvature, the pressure difference in the swollen layer between x_c and $x_c+\phi x$ can be calculated as

$$\Delta P = P_d(x_c) - P_d(x_c + \Delta x) \qquad (3)$$

For $W(x) \;) \; h_0 \sin(\omega x)$, the crest of the sine wave lies at $x_c = \pi/2\omega$.

(32) Bird, R. B.; Stewart, W.E.; Lightfoot, E. N. *Transport Phenomena*; John Wiley & Sons: New York, 1960.
(33) Geankoplis, C. J. *Transport Processes and Unit Operations*, 3rd ed.; Prentice Hall: Englewood Cliffs, NJ, 1993.

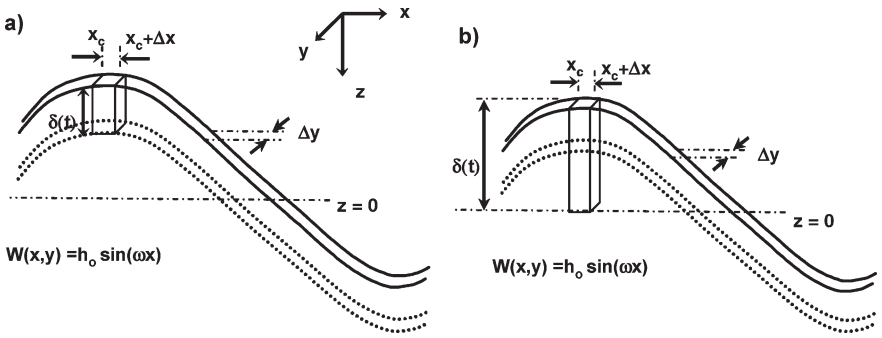

Figure 10. Schematic showing the sinusoidal surfaces and control volumes considered in the falling-film model.

The pressure decrease described using eq 3 leads to mass transfer within the solvent-swollen layer in the positive x direction away from x_c at the sinusoidal crest. The resulting problem is analogous to a falling film [32,33] and can be solved by performing a momentum balance in the x direction with a no-slip boundary condition at z) δ and a zero shear boundary condition at z) 0. With these boundary conditions, the falling film model can be used to relate fluid velocity in the x direction to z, the depth within the swollen layer

$$v_x) \frac{\Delta P \delta^2}{2\mu \Delta x}\left(1 - \frac{z^2}{\delta^2}\right) \quad (4)$$

By integrating eq 4 over the thickness of the swollen layer and over an arbitrary distance in the y direction Δy, the volumetric flow rate is calculated as

$$q) \int_0^{\Delta y}\int_0^{\delta} v_x \, dz \, dy \quad (5)$$

Substituting v_x from eq 4 into eq 5 and integrating yields

$$q) \frac{\Delta P \delta^3 \Delta y}{3\mu \Delta x} \quad (6)$$

The swollen layer thickness will increase due to the solvent front propagating further into the material, but it will also decreases due to mass flow away from the wave crest. These two competing effects are accounted for by performing a mass balance on a control volume shown in Figure 10a that is defined by Δx, Δy, and δ:

$$\text{(accumulation)}) \text{(in)} - \text{(out)}$$

$$\frac{d\delta}{dt}\Delta x \Delta y) v_f \Delta x \Delta y - q \quad (7)$$

In this expression, accumulation of mass is accounted for by allowing the control volume to change shape. Note that, due to the symmetry of the sinusoidal surface, fluid flow is only permitted in the positive x direction. A similar mass balance can be written using the control volume shown in Figure 10b:

$$\frac{dh}{dt}\Delta x \Delta y) - q \quad (8)$$

In this case, the rate of change in the surface amplitude only depends on the fluid flow term.

The time dependence of the sinusoidal amplitude h(t) and the swollen layer thickness δ(t) can be solved by integrating eqs 7 and 8, where initial conditions are given by h(0)) h_0 and δ(0)) 0. In its final form, our model only contains three adjustable parameters: surface tension, viscosity of the swollen layer, and the solvent front velocity. We assumed a surface tension of 40 dyn/cm; this is a typical value for organic liquids (DMSO has a surface tension of 43.54 dyn/cm at 20 °C [34]). The remaining two parameters, the swollen layer viscosity and the solvent front velocity, were systematically varied, and eqs 7 and 8 were integrated to generate the least-squares fits shown in Figure 9 (solid lines). The amplitude decay dynamics were found to be much more sensitive to the frontal velocity than to the swollen layer viscosity. Rather remarkable least-squares fits were obtained for experiments conducted at gas flow rates of 50 and 100 cm ^{3}/min (Figure 9a,b). The upward-sloping lines in Figure 9 correspond to the thickness of the swollen layer at the crest of a sinusoids δ(t). At gas flow rates of 50 and 100 cm ^{3}/min the swollen layer is less than 5 μm thick when most of the surface smoothing occurs. This validates the assumption that mass transfer at the crest of the sinusoid is predominately in the x direction.

For experiments conducted at 200 cm ^{3}/min, the falling film model only qualitatively describes experimental data. While the model is effective in describing the sigmoid shape of the amplitude decay curve, it fails to describe the frequency dependence of the decay. This is apparent by examining the data shown in Figure 9c. To illustrate this shortcoming, the model has been forced to fit the surfaces with high frequencies by choosing v_f) 0.4 μm/min and μ) 10^4 P. Consequently, the model predicts slower smoothing over the long-wavelength sinusoidal surface than is observed experimentally.

One possible reason the falling film model fails at 200 cm^3/min is that the swollen layer may be significantly thicker due to a higher solvent-front velocity. Whereas the model only considered mass transfer in the x direction, a thick swollen layer would permit viscous flow in both the x and z directions. Furthermore, under forced convection conditions, several factors can complicate the relationship between gas composition, gas flow rate, and the time dependence of the swollen layer thickness δ(t). Laminar flow of saturated solvent vapor across the absorbent polymer surface may lead to a boundary layer that becomes less saturated with solvent. This implies that the rate of solvent uptake may also depend on the lateral (x and y in Figure 10) position. Also, channel geometry and surface perturbations in the poly(amic acid) film may create two- or three-dimensional gas velocity fields that complicate laminar flow. To properly address these issues, we plan on obtaining experimental mass transfer coefficients under different flow conditions in well-defined channel geometries.

If the solvent front velocity is large enough, then we no longer need to think about a swollen layer; rather, we will consider the smoothing of a viscous liquid film. A few

(34) Dean, J. A. Lange's Handbook of Chemistry , 13th ed.; McGraw-Hill: New York, 1985.

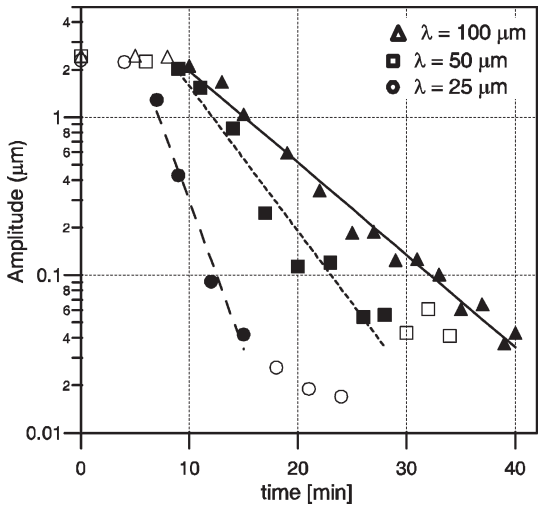

Figure 11. Log of surface amplitude vs time for all three periods for three sinusoidal surfaces plotted as a function of solvent exposure time. The solid and dashed lines are linear fits to the selected data for each surface where the induction and tail times have been ignored. The linear fits have slopes of - 0.13, - 0.21, and - 0.43 min $^{-1}$ for λ) 100, 50, and 25 μm, respectively.

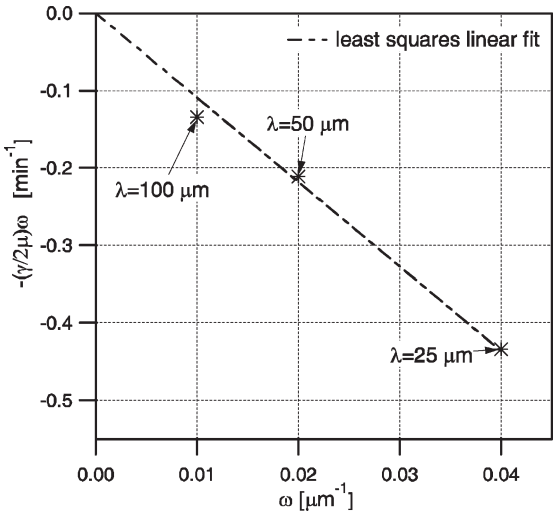

Figure 12. The quantity - Aω) - (γ/2η)ω determined from linear fits to the data in Figure 9 plotted against surface frequency for the sinusoidal PAA coatings. The dotted line is a linear least-squares fit through the origin and suggests that γ/2η) 1.09 × 10^{-5} m/min^{-1}.

decades ago, Mullins addressed the smoothing of viscous films through a more generalized, mathematical explanation of surface flattening. [35] Part of his analysis conveniently considered the capillary relaxation of a planar 1-D sinusoidal surface W$_0$) a sin(ωx), where ω) 2π/λ. The surface amplitude was found to decrease exponentially with time, i.e.

$$W(t) \;)\; W_0 \exp[-(F\omega + A\omega^2 + D\omega^3 + B\omega^4)t] \quad (9)$$

where the coefficients F, A, D, and B are associated with contributions from viscous flow, evaporation - condensation, volume diffusion, and surface diffusion. Mullins explained the first term (for viscous flow) by solving the Navier - Stokes equations for an incompressible fluid, ignoring inertial terms. His main assumptions (see Mullins [35] for details) were (1) the surface is initially nearly flat, (2) there is zero shear stress at the free surface, (3) the pressure immediately underneath the surface is given by eq 1, and (4) there is no fluid flow at infinite film depths. Mullins' result for relaxation by viscous flow was that the position and time dependence of the surface height W(x,t) is described by

$$\partial W/\partial t \;)\; -F\omega W \quad (10)$$

where F) - γ/2η and η is the fluid viscosity which was also assumed constant. Equation 10 relates the amplitude rate of decay to the frequency of the surface. Following integration of eq 10, one obtains

$$\ln(W) \;)\; -Fwt + c \quad (11)$$

where c is an integration constant. Accordingly, Mullins' model predicts that the natural logarithm of amplitude should be related linearly to time and frequency by a constant F) γ/2η.

Figure 11 shows the log of the amplitude decay for the data acquired at 200 cm ^{3}/min plotted against time. Data are nearly linear at intermediate exposure times. Linear regression fits were obtained for selected data denoted by darkened symbols in Figure 11. If one were to interpret the data in Figure 11 in the context of Mullins' model, then, according to eq 10, the slopes obtained from the regression analysis should be proportional to the surface frequency ω) 2π/λ by a factor of F) γ/2η. The slopes of these lines are then plotted against frequency in Figure 12. The data in Figure 12 can be fit with a linear fit through the origin, suggesting that γ/2η ≈ 1.09 × 10^{-5} m/min^{-1}. This single parameter can be used to describe all the data in Figure 11, and the data acquired at gas flow rates of 200 cm ^{3}/min suggest that the mechanism of mass transport accompanying smoothing is bulk viscous flow. If one assumes a surface tension of 40 dyn/cm, the film's bulk viscosity is predicted to be ? 10^5 P. This estimate of viscosity is higher than the falling-film model by a factor of 10.

In principle, Mullins' analysis can be taken one step further by applying it to the smoothing of an arbitrarily rough surface. Since any function can be approximated by a Fourier series, i.e.

$$f(x) \;)\; \sum_k A_k e^{i\omega_k} \quad (12)$$

then the Fourier coefficient |A$_k$| can be thought of as the amplitude of the periodic function that contributes to the surface at a frequency ω$_k$. Along these lines, the Fourier transform was calculated for the arbitrarily rough surface smoothed at higher flow rates (250 mL/min) described in Figure 5. The logrithom of A$_k$ is plotted against time for a series off requencies in Figure 13. This plot is analogous to that shown in Figure 11. The data are treated as linear at intermediate exposure times.

Linear regression was performed on data in this regime s points were only considered with Fourier coefficients between 90% and 10% of their initial value. (These points are denoted by symbols in Figure 13.) Figure 14 shows the calculated slopes graphed against frequency. The linear fit at low frequencies suggests that this analysis is suitable for an arbitrarily rough surface. It is somewhat surprising that this scaling works for the arbitrarily rough surface because the surface is no longer unidimensional. The smoothing ofi solated 2-D defect should be faster since viscous flow can occur in more than one direction. We are beginning to explore this phenomenon by smoothing polymers over isolated 2D hemispherical defects.

(35) Mullins, W. W. J. Appl. Phys. 1959 , 30, 77 - 83.

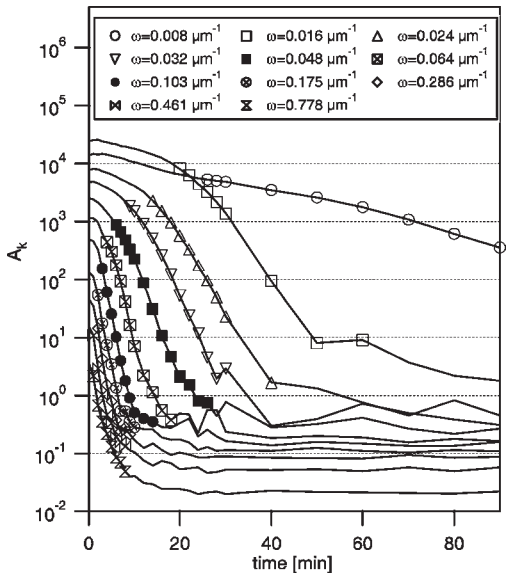

Figure 13. Log of Fourier components A_k's for the arbitrarily rough surfaces shown in Figure 5 plotted against solvent exposure time. Each data set represents a different Fourier frequency ω_k. Data are linear at intermediate solvent exposure times; the symbols denote the data points that were used for linear fits.

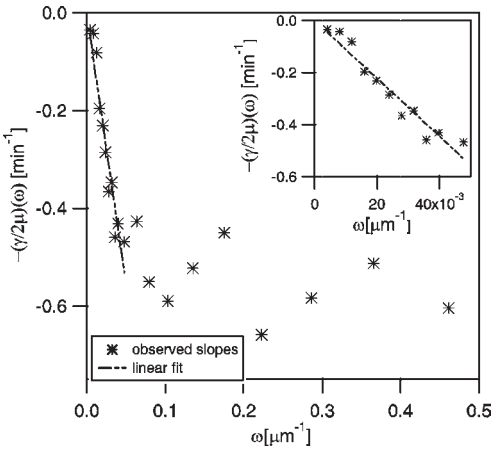

Figure 14. The quantity - Aω) - (γ/2η)ω determined from linear fits to the data in Figure 11 plotted against surface frequency for the arbitrarily rough PAA coating. The dashed line fits data at early times and suggests that - (γ/2η)) 1.09 × 10⁻⁵ m/min⁻¹.

The data in Figure 14 indicate that the rate of surface smoothing is independent off requency for ω greater than a critical frequency $\omega_c \approx 0.05$ μm⁻¹. In Figure 14, above ω_c, the quantity (- γ/2η)ω is about 0.6 min⁻¹ and is nearly constant. Perhaps, at these high frequencies, surface smoothing does not depend on the viscous flow of the swollen layer; instead, smoothing is limited by the dynamics off rontal diffusion as described by Thomas and Windle. [26] If this were true, the rate of smoothing would be ultimately limited by the rate of polymer relaxation occurring in the glassy state as chains are swollen with solvent molecules. On the other hand, at high frequencies there appear to be shorter induction times (see Figure 13), which would suggest varying rates of swelling. One explanation for this observation is that surfaces with high frequencies have nonnegligible edge surface areas that may increase the rate ofl ocal solvent sorption. High and narrow surface protrusions absorb solvent faster and begin smoothing before wider defects.

The solvent-vapor surface smoothing examined here can be compared to surface smoothing observed in annealing experiments. On the basis of the preceding discussion, in an annealing experiment one would expect mass transfer to be dominated by viscous flow; however, this is not always the case. Goh et al. [9] have studied changes in the surface topology during annealing ofl atex films using AFM techniques. They reported on the flattening dynamics of a highly ordered array of spherical poly(butyl methacrylate) latex particles (d) 337 nm) by monitoring the peak-to-valley surface modulation as a function of time. The decay of the peak-to-valley corrugations occurs much faster than an exponential decay. The authors present a Brownian diffusion model that agrees well with their data; the determined diffusion coefficients are 4 orders of magnitude greater than the polymers in the interior of the film. Li et al. [1] have applied Mullins' formalism to examine the annealing of higher molecular weight polystyrene and poly(methyl methacrylate) thin films that were spun-cast over laterally structured silicon substrates. The length scale of their features is roughly an order of magnitude smaller than those discussed in this paper. The authors ruled out viscous flow as the governing transport mechanism, and instead, their data confirm that surface flattening is governed by

$$\ln(W)) - B\omega^4 t \qquad (13)$$

where B is the coefficient in eq 9 that is associated with the surface diffusion transport mechanism. The authors determined values obtained for B by fitting amplitude vs time data for two different surface frequencies, and from B , the surface diffusion coefficients of entangled polymer melts were then calculated and were in agreement with independent experimental evidence. These two studies point out that during annealing diffusion may dominate mass transport near surfaces or within thin films. The present study involving solvent swelling represents an example where mass transfer occurs near the surface at early times and well beneath the surface at later times.

Conclusions

We have found that DMSO sorption into vapor-deposited PAA can be described by case II diffusion. Mass-uptake and SIMS data confirm that penetrating solvent molecules form a well-defined solvent propagation front, behind which is a layer with a constant solvent concentration and a constant polymer viscosity. Subsequently, as the solvent front progresses deep enough into the material, surface smoothing follows and is driven by surface tension and retarded by viscous forces. The rate of surface smoothing depends on both gas flow rate and surface frequency. At gas flow rates of 50 and 100 cm [3]/min, for the frequencies studied, surface smoothing data are in remarkable agreement with a two-parameter falling film model. In the falling-film model flow is permitted only inside a time-dependent swollen polymer layer. At gas flow rates of 200 cm [3]/min surface smoothing may involve bulk viscous flow of material, and data can be described using the single-parameter viscous flow term from Mullins' model. Future efforts will be directed at understanding how temperature and flow conditions influence sorption and smoothing phenomena.

Acknowledgment. This work was performed under the auspices of the U.S. Department of Energy by the University of California Lawrence Livermore National Laboratory under Contract W-7405-Eng-48.